

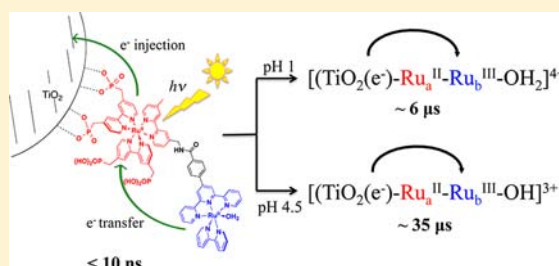
Photoinduced Electron Transfer in a Chromophore–Catalyst Assembly Anchored to TiO₂

Dennis L. Ashford, Wenjing Song, Javier J. Concepcion, Christopher R. K. Glasson, M. Kyle Brennaman, Michael R. Norris, Zhen Fang, Joseph L. Templeton, and Thomas J. Meyer*

Department of Chemistry, University of North Carolina at Chapel Hill, CB 3290, Chapel Hill, North Carolina 27599-3290, United States

S Supporting Information

ABSTRACT: Photoinduced formation, separation, and buildup of multiple redox equivalents are an integral part of cycles for producing solar fuels in dye-sensitized photoelectrosynthesis cells (DSPECs). Excitation wavelength-dependent electron injection, intra-assembly electron transfer, and pH-dependent back electron transfer on TiO₂ were investigated for the molecular assembly $[(\text{PO}_3\text{H}_2\text{-CH}_2\text{-bpy})_2\text{Ru}_a(\text{bpy-NH-CO-trpy})\text{Ru}_b(\text{bpy})(\text{OH}_2)]^{4+}$ ($[\text{TiO}_2\text{-Ru}_a^{\text{II}}\text{-Ru}_b^{\text{II}}\text{-OH}_2]^{4+}$; $(\text{PO}_3\text{H}_2\text{-CH}_2)_2\text{-bpy} = ([2,2'\text{-bipyridine}]\text{-4,4'\text{-diylbis(methylene)})\text{diphosphonic acid}$; $\text{bpy-ph-NH-CO-trpy} = 4\text{-}([2,2':6',2''\text{-terpyridin}]\text{-4'\text{-yl})\text{-N-}((4'\text{-methyl-}[2,2'\text{-bipyridin}]\text{-4-yl)-methyl) benzamide$); $\text{bpy} = 2,2'\text{-bipyridine}$). This assembly combines a light-harvesting chromophore and a water oxidation catalyst linked by a synthetically flexible saturated bridge designed to enable long-lived charge-separated states. Following excitation of the chromophore, rapid electron injection into TiO₂ and intra-assembly electron transfer occur on the subnanosecond time scale followed by microsecond–millisecond back electron transfer from the semiconductor to the oxidized catalyst, $[\text{TiO}_2(\text{e}^-)\text{-Ru}_a^{\text{II}}\text{-Ru}_b^{\text{III}}\text{-OH}_2]^{4+} \rightarrow [\text{TiO}_2\text{-Ru}_a^{\text{II}}\text{-Ru}_b^{\text{II}}\text{-OH}_2]^{4+}$.



INTRODUCTION

In producing solar fuels by artificial photosynthesis, as in natural photosynthesis, a key requirement is the integration of UV–visible–near IR light absorption with a sequence of electron transfer events to drive the component half reactions: water oxidation into protons and oxygen and reduction of CO₂ to CO, other oxygenates, or hydrocarbons.^{1–5} Water oxidation in photosystem II (PSII) occurs through a series of four sequential single-photon, single-electron transfer events, which activate the multielectron CaMn₄ catalyst in the oxygen-evolving complex (OEC) toward water oxidation and O₂ release.^{6–10} Activation and water oxidation are driven by light absorption at an “antenna complex”, followed by sensitization of chlorophyll P₆₈₀ that initiates a series of electron transfer events resulting in oxidative activation of the OEC.^{11–16} Water oxidation is coupled to reduction of plastoquinone to plastoquinol, ultimately with delivery of reductive equivalents to photosystem I and further to the Calvin cycle for light-driven CO₂ reduction.^{17–19}

Photosystem II is a highly complex, membrane-bound assembly that has remained unchanged over 2.4 B years.^{6,7,20,21} Successful strategies for artificial photosynthesis and large-scale solar fuel production will require straightforward approaches and simple designs. One approach, illustrated in Figure 1, is a photoelectrochemical approach based on dye-sensitized photoelectrosynthesis cells (DSPECs).^{16,22–25} The figure illustrates a photoanode for water oxidation based on a chromophore–catalyst assembly surface-bound to a wide band

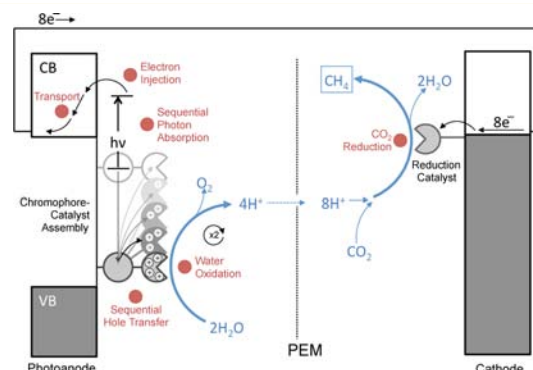


Figure 1. Schematic drawing of a dye-sensitized photoelectrosynthesis cell (DSPEC) based on a chromophore–catalyst assembly on TiO₂ as the photoanode.

gap metal oxide semiconductor, typically TiO₂. Chromophore excitation at the surface is followed by excited-state electron injection into the conduction band of the semiconductor with the reductive equivalents delivered to a cathode for catalytic water reduction to hydrogen or CO₂ reduction to CH₄, the reaction illustrated in Figure 1. The DSPEC approach is closely related to dye-sensitized solar cells (DSSCs), but the target is the production and collection of oxygen and a high-energy fuel

Received: August 24, 2012

Published: October 27, 2012

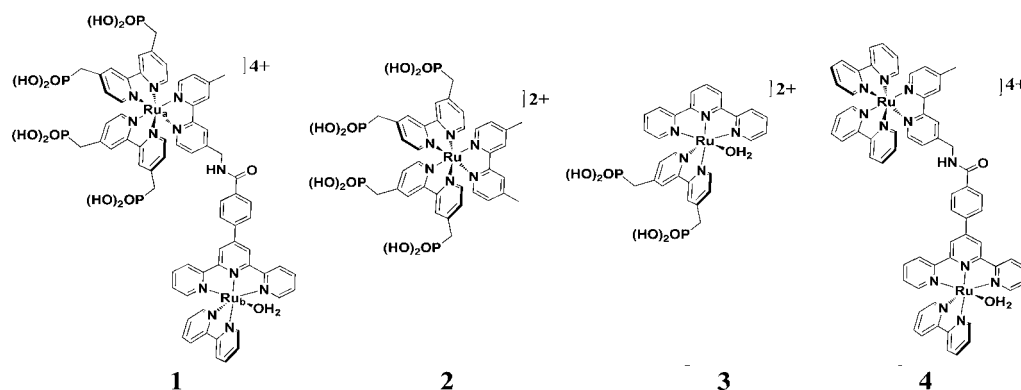


Figure 2. Structures of the assembly $[(4,4'-(\text{PO}_3\text{H}_2\text{-CH}_2)_2\text{-bpy})_2\text{Ru}_a(\text{bpy-NH-CO-trpy})\text{Ru}_b(\text{bpy})(\text{OH}_2)]^{4+}$ (**1**), chromophore $[\text{Ru}(4,4'-(\text{PO}_3\text{H}_2\text{-CH}_2)_2\text{bpy})_2(\text{dmb})]^{2+}$ (**2**), catalyst $[\text{Ru}(\text{trpy})(4\text{-PO}_3\text{H}_2\text{-CH}_2\text{-bpy})(\text{OH}_2)]^{2+}$ (**3**), and the nonphosphonated assembly $[(\text{Ru}(\text{bpy})_2(\text{bpy-ph-NH-CO-trpy})\text{Ru}(\text{bpy})(\text{OH}_2))]^{4+}$ previously reported.³³

at spatially separated electrodes rather than a photopotential and photocurrent.^{3,26,27}

Key elements in DSPEC designs include light absorption throughout the solar spectrum ($\lambda < 1000$ nm for water splitting by single-photon absorption), excited-state electron transfer, utilization of internal free energy gradients to drive long-range electron and proton transfer, and stepwise activation of catalysts for carrying out multiple electron–multiple proton catalysis.^{3,28,29} In a successful photoanode design, the water oxidation catalyst and chromophore must be in sufficiently close proximity for rapid and efficient electron transfer oxidation of the catalyst to occur following chromophore excitation and electron injection into the conduction band of the semiconductor. At the same time, the intramolecular structure should inhibit back electron transfer from the electrode to the oxidatively activated catalyst on a time scale that allows for the initial step in O–O bond formation.^{3,30–32}

Exploitation of this strategy requires a versatile synthetic approach for linking chromophores with water oxidation catalysts to control intramolecular electron transfer rates. The strategy must be compatible with the presence of surface binding functional groups, such as phosphonic acids. These are required for surface stability in aqueous environments and for creating electronic coupling pathways from the excited state of the chromophore to the conduction band or acceptor levels of the metal oxide electrodes.^{34–36}

We previously reported on electrocatalytic water oxidation by the assemblies $[(\text{bpy})_2\text{Ru}^{\text{II}}(\text{bpm})\text{Ru}^{\text{II}}(\text{trpy})(\text{OH}_2)]^{4+}$ and $[(\text{bpy})_2\text{Ru}^{\text{II}}(\text{bpm})\text{Ru}^{\text{II}}(\text{Mebimpy})(\text{OH}_2)]^{4+}$ (bpy = 2,2'-bipyridine; bpm = 2,2'-bipyrimidine; trpy = 2,2':6',2''-terpyridine; Mebimpy = 2,6-bis(1-methyl-benzimidazol-2-yl)pyridine) both in solution and, as phosphonate derivatives, on metal oxide electrodes.³⁷ We have also reported on photoinduced electron injection and back electron transfer rates for the assembly $[(\text{dcb})_2\text{Ru}(\text{bpy-Mebim}_2\text{-py})\text{Ru}(\text{bpy})(\text{OH}_2)](\text{OTf})_4$ (dcb = 4,4'-dicarboxylic acid-2,2'-bipyridine; bpy-Mebim₂-py = 2,2'-(4-methyl-[2,2':4',4''-terpyridine]-2'',6''-diyl)bis(1-methyl-1H-benzo[d]imidazole) anchored to TiO₂ by carboxylic acid linkers.³⁸ For the latter, low electron injection efficiencies were attributed to a lowest metal-to-ligand charge transfer (MLCT) excited state localized on the conjugated bridging ligand leading to competitive, deleterious nonradiative decay.

Recently, we also reported a general approach for the synthesis of chromophore–catalyst assemblies based on an amide-linkage strategy in the assembly $[(\text{Ru}(\text{bpy})_2(\text{bpy-NH-}$

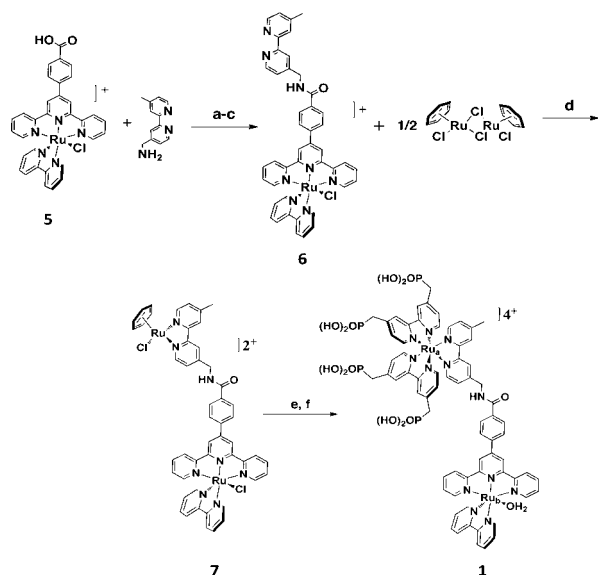
$\text{CO-trpy})\text{Ru}(\text{bpy})(\text{OH}_2)]^{4+}$ (bpy-NH-CO-trpy = 4-([2,2':6',2''-terpyridin]-4'-yl)-N-((4'-methyl-[2,2'-bipyridin]-4-yl)methyl)methyl) (**4**).³³ In this strategy, the bridging benzamide introduces a unit of saturation between the linked chromophore and catalyst where the separate properties of the chromophore and catalyst are retained.³³ Generically, saturated amide links are appealing in providing a basis for controlling the extent of electronic coupling by synthetic modification and, with it, rates of intramolecular electron transfer.

We report here on the photophysical dynamics of the phosphonic acid-derivatized, amide-linked assembly, $[(\text{PO}_3\text{H}_2\text{-CH}_2)_2\text{-bpy})_2\text{Ru}_a(\text{bpy-NH-CO-trpy})\text{Ru}_b(\text{bpy})(\text{OH}_2)]^{4+}$ ($(\text{PO}_3\text{H}_2\text{-CH}_2)_2\text{-bpy} = ([2,2'\text{-bipyridine}]_{-4,4'}\text{-diyl-bis(methylene)diphosphonic acid})$ (**1**) on TiO₂ (TiO₂-1; [TiO₂-Ru^{II}-Ru^{II}-OH₂]⁴⁺) which is one of a limited number of phosphonate-derivatized chromophore–catalyst assemblies reported with metal oxide attachment.³⁷ A general synthetic procedure is described, as are the characterization and surface binding of the assembly and its spectroscopic, electrochemical, and photophysical characterization. Interfacial dynamics of the assembly on TiO₂, injection yields, and back electron transfer rates are compared with the constituent monomers $[\text{Ru}((\text{PO}_3\text{H}_2\text{-CH}_2)_2\text{-bpy})_2(\text{dmb})]^{2+}$ (**2**) (dmb = 4,4'-dimethyl-2,2'-bipyridine) and $[\text{Ru}(\text{trpy})((\text{PO}_3\text{H}_2\text{-CH}_2)_2\text{-bpy})(\text{OH}_2)]^{2+}$ (**3**) (Figure 2).

RESULTS

Synthesis. In a modification of the approach taken in the synthesis of **4**, the phosphonate-derivatized chromophore in **1** was synthesized by use of the $[\text{Ru}(\text{bpy})(\text{Bz})(\text{Cl})]^+$ analogue, $[\text{Ru}(\text{bpy})(\text{Cl})(\text{trpy-CO-NH-bpy})\text{Ru}(\text{Bz})(\text{Cl})](\text{Cl})(\text{PF}_6)$ (**7**) (Scheme 1). This strategy was used because of the limited solubility of the phosphonated chromophore under conditions relevant for amide coupling in dimethylformamide solution.³³ The precursor to **7** is the product of an amide coupling between the water oxidation catalyst precursor $[\text{Ru}(\text{bpy})(4-([2,2':6',2''\text{-terpyridin}]-4'\text{-yl})\text{benzoic acid})(\text{Cl})](\text{Cl})$ (**5**) and (4'-methyl-[2,2'-bipyridin]-4-yl)methanamine to give $[\text{Ru}(\text{bpy-ph-NH-CO-trpy})(\text{bpy})(\text{Cl})]^+$ (**6**) in high yields (see Experimental Section). **6** can be used without further purification because **7** precipitates cleanly from the reaction mixture, leaving both unreacted **6** and (4'-methyl-[2,2'-bipyridin]-4-yl)-methanamine in solution.

Two-dimensional (2D) NMR analysis by COSY was utilized to identify the methylene protons and NH proton in **7** and

Scheme 1. Synthesis of **1**^a

^aReagents and conditions: a) SOCl_2 , reflux, 4 h. b) (4'-Methyl-[2,2'-bipyridin]-4-yl)methanamine, DMF, DIPEA, 100 °C, overnight. c) NH_4PF_6 . d) MeOH, reflux, overnight. e) CH_2Cl_2 , HOTf. f) 2 equiv $(\text{PO}_3\text{H}_2\text{-CH}_2)_2\text{bpy}$, ethylene glycol, 120 °C, 5 h.

$[\text{Ru}(\text{bpy})(\text{OTf})(\text{trpy-CO-NH-bpy})\text{Ru}(\text{Bz})(\text{OTf})](\text{OTf})_2$ (**8**) (Figure 3). The shifts for the NH proton, as expected, are dependent on the solvent but were typically found between δ 8.5–9.5 ppm. The methylene protons were between δ 4.8–4.9 ppm, and the chemical shifts were relatively independent of solvent. The diastereotopic nature of the methylene protons in **7** was evident since they appear as an AB pattern giving a pair of doublets (Figures 3 and S3 in Supporting Information [SI]). This analysis was not possible for **1** because of its limited solubility in solvents other than D_2O , in which the methylene protons are masked by the solvent.

The $[\text{Ru}(\text{Bz})(\text{Cl})(\text{bpy-NH-CO-})]$ site in **7** is kinetically inert to further substitution and binding. Both the bound chloro ligand and the chloride counterion in **7** can be removed by treatment with triflic acid (HOTf, $\text{OTf}^- = \text{trifluoromethanesulfonate anion}$) to give the triflate derivative, **8**. The triflate derivative undergoes substitution with added 4,4'-($\text{PO}_3\text{H}_2\text{-CH}_2$)₂bpy in ethylene glycol, Scheme 1. The final substitution step, Scheme 1, was followed by UV–visible measurements

where the characteristic $[\text{Ru}(\text{bpy})_3]^{2+}$ -based absorptions for the $[(\text{PO}_3\text{H}_2\text{-CH}_2)_2\text{bpy}]_2\text{-Ru}_a(\text{bpy-NH-CO-})$ fragment grow at $\lambda_{\text{max}} \approx 472$ nm as the reaction proceeds. There were no further spectral changes after 5 h (Figure S7 [SI]).

Electrochemistry. In cyclic voltammograms of **1** immobilized on planar fluoride-doped tin oxide (FTO) at pH = 6.0, pH-dependent waves appear for the $[\text{Ru}_a^{\text{II}}\text{-Ru}_b^{\text{III}}\text{-OH}]^{4+}/[\text{Ru}_a^{\text{II}}\text{-Ru}_b^{\text{II}}\text{-OH}_2]^{4+}$, $[\text{Ru}_a^{\text{II}}\text{-Ru}_b^{\text{IV}}\text{=O}]^{4+}/[\text{Ru}_a^{\text{II}}\text{-Ru}_b^{\text{III}}\text{-OH}]^{4+}$, and $[\text{Ru}_a^{\text{III}}\text{-Ru}_b^{\text{IV}}\text{=O}]^{5+}/[\text{Ru}_a^{\text{II}}\text{-Ru}_b^{\text{IV}}\text{=O}]^{4+}$ couples at $E_{1/2} = 0.71$ V, 0.83 V, and 1.23 V (vs NHE), respectively (Figure 4). In contrast to **4** in solution, the $[\text{Ru}_a^{\text{III}}\text{-}]^{5+}/[\text{Ru}_a^{\text{II}}\text{-}]^{4+}$ couple is also (weakly) pH-dependent (Figures 4 and S8 [SI]). $\text{p}K_a$ values for $[\text{Ru}_a^{\text{II}}\text{-Ru}_b^{\text{II}}\text{-OH}_2]^{4+}$ and $[\text{Ru}_a^{\text{II}}\text{-Ru}_b^{\text{III}}\text{-OH}_2]^{5+}$ were determined previously for **4** in solution (Figure 4).^{33,39}

The pH-dependent results are summarized in the $E_{1/2}$ ($\sim E^{\circ'}$: $E^{\circ'}$ is the formal potential) vs pH (Pourbaix) diagram in Figure 4. As shown in the figure, the slopes of the $E_{1/2}$ /pH plots between pH = 1 and pH = 8 are ~ 74 mV/pH unit, larger than the 59 mV/pH unit predicted by the Nernst equation. The pH dependence for the nominally pH independent $[\text{Ru}_a^{\text{III}}\text{-}]^{5+}/[\text{Ru}_a^{\text{II}}\text{-}]^{4+}$ couple is ~ 13 mV/pH unit. Spectroelectrochemical results on conductive nano-ITO (ITO = tin-doped indium oxide) derivatized with **1** show an oxidation of the catalyst moiety $[\text{Ru}_a^{\text{II}}\text{-Ru}_b^{\text{II}}\text{-OH}_2]^{4+}$ to give $[\text{Ru}_a^{\text{II}}\text{-Ru}_b^{\text{III}}\text{-OH}_2]^{5+}$ followed by a second oxidation of the catalyst that overlaps with the oxidation of the chromophore to give $[\text{Ru}_a^{\text{III}}\text{-Ru}_b^{\text{IV}}\text{=O}]^{5+}$ (Figure S13 [SI]).

Transient Absorption. The absorption spectrum of **1** in water at 25 °C in the visible is dominated by a MLCT absorption centered at $\lambda_{\text{max}} \approx 472$ nm. This feature results from overlapping MLCT absorptions at $[\text{Ru}_a^{\text{II}}\text{-}]^{4+}$ and $[-\text{Ru}_b^{\text{II}}\text{-OH}_2]^{4+}$ which are unperturbed compared to the constituents due to weak electronic coupling across the saturated amide link (Figure 6).³³

Interfacial electron transfer dynamics of TiO_2 derivatized with $[\text{Ru}_a^{\text{II}}\text{-Ru}_b^{\text{II}}\text{-OH}_2]^{4+}$ (**1**), $[\text{Ru}^{\text{II}}]^{2+}$ (**2**), and $[\text{Ru}^{\text{II}}\text{-OH}_2]^{2+}$ (**3**) were investigated by nanosecond transient absorption measurements. Initial electron injection into the TiO_2 conduction band following MLCT excitation was $>10^8$ s⁻¹, too rapid to monitor on the time scale of the experiment (10 ns instrumental time resolution).

Transient absorption difference spectra following 532 nm excitation are shown in Figure 5. There is a resemblance in absorption features in the transient spectra of $[\text{TiO}_2\text{-Ru}_a^{\text{II}}\text{-}]$

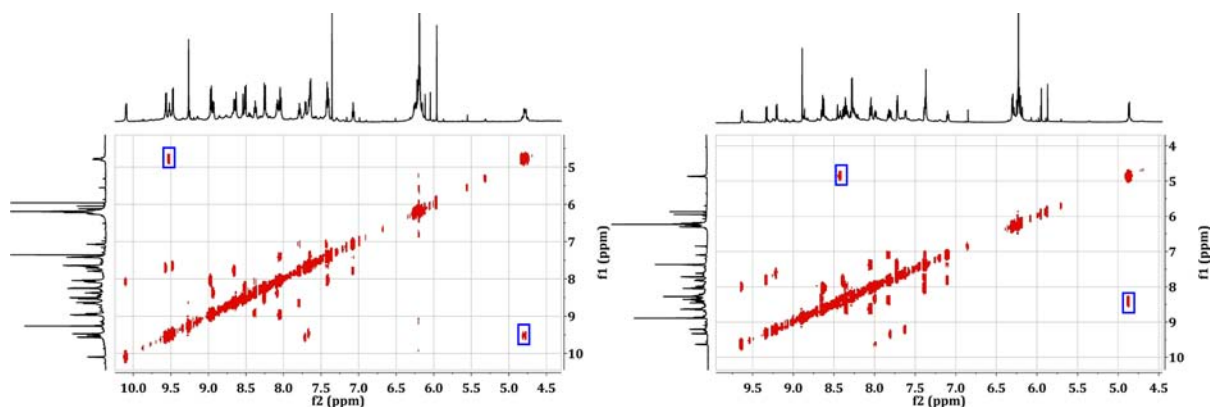


Figure 3. (Left) COSY NMR of **7** in d_6 -DMSO. (Right) COSY NMR of **8** in CD_3CN . The cross peaks for each of the diastereotopic methylene protons and the NH proton for both complexes are highlighted in blue.

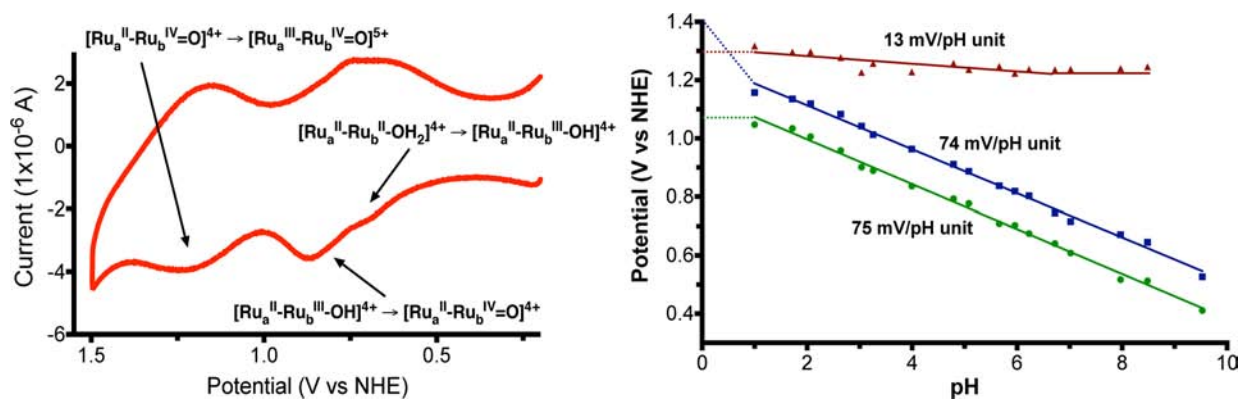
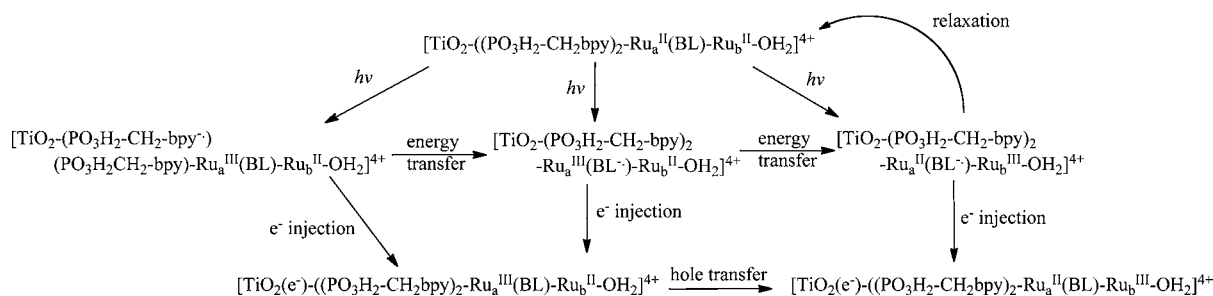


Figure 4. (Left) Cyclic voltammogram for **1** at pH = 6.0 (0.1 M phosphate, 0.5 M KNO₃) at 100 mV/s on FTO. (Right) $E_{1/2}$ /pH diagram of **1** on FTO. $E_{1/2}$ values were obtained as peak current maxima in differential pulse voltammograms. The solid lines are best fits of the variation in $E_{1/2}$ values with pH for the $[-\text{Ru}_b^{\text{III}}-\text{OH}]^{4+}/[-\text{Ru}_b^{\text{II}}-\text{OH}_2]^{4+}$ (green), $[-\text{Ru}_b^{\text{IV}}=\text{O}]^{4+}/[-\text{Ru}_b^{\text{III}}-\text{OH}]^{4+}$ (blue), and $[\text{Ru}_a^{\text{III}}-\text{O}]^{5+}/[\text{Ru}_a^{\text{II}}-\text{O}]^{4+}$ (red) couples, at 23 °C in 0.5 M KNO₃ and 0.1 M buffer.

Scheme 2. Summary of Possible Electron and Energy Transfer Events Following Excitation of TiO₂-1^a



^aNote that in the bridging ligand, BL = bpy-NH-CO-trpy, the lowest π^* level is trpy based.

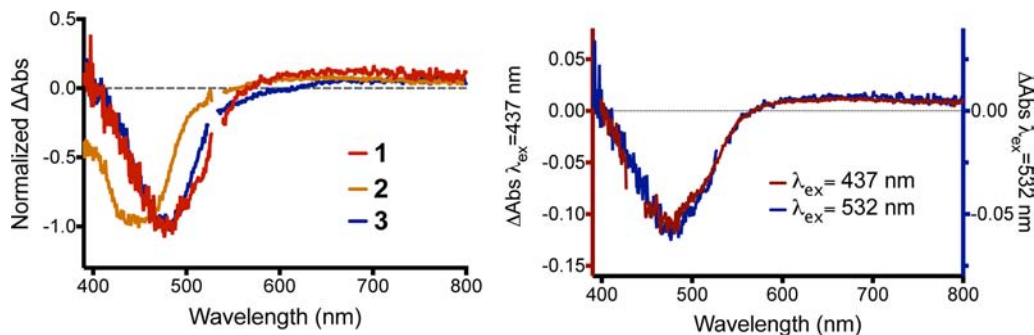
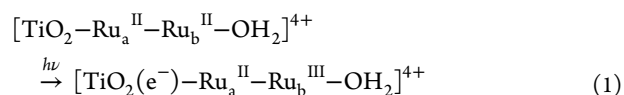


Figure 5. (Left) Nanosecond transient absorption difference spectra obtained at 20 ns on TiO₂ (6 μm transparent film)-derivatized electrodes at surface coverages: **1** (4.4×10^{-8} mol cm⁻², red), **2** (5.8×10^{-8} mol cm⁻², orange), and **3** (9.1×10^{-8} mol cm⁻², blue) following 532 nm laser (5.2 mJ) excitation. Spectra are normalized at the bleach maxima for comparison purposes. (Right) Transient spectrum for **1** (4×10^{-8} mol cm⁻²) at 20 ns following 532 nm (5.2 mJ, blue) and 437 nm (3 mJ, red) excitation on TiO₂. In 0.1 M HClO₄ at room temperature.

$\text{Ru}_b^{\text{II}}-\text{OH}_2]^{4+}$ (TiO₂-1) and $[\text{TiO}_2-\text{Ru}^{\text{II}}-\text{OH}_2]^{2+}$ (TiO₂-3) with a maximum bleach at 480 nm. This feature points to the formation of $[\text{TiO}_2(\text{e}^-)-\text{Ru}_a^{\text{II}}-\text{Ru}_b^{\text{III}}-\text{OH}_2]^{4+}$ following excitation of TiO₂-1 at 20 ns. This is consistent with MLCT excitation of $[\text{TiO}_2-\text{Ru}_a^{\text{II}}-\text{Ru}_b^{\text{II}}-\text{OH}_2]^{4+}$ followed by rapid injection and subnanosecond, intra-assembly oxidation of $[\text{TiO}_2(\text{e}^-)-\text{Ru}_a^{\text{III}}-\text{Ru}_b^{\text{II}}-\text{OH}_2]^{4+}$ to $[\text{TiO}_2(\text{e}^-)-\text{Ru}_a^{\text{II}}-\text{Ru}_b^{\text{III}}-\text{OH}_2]^{4+}$, eq 1 and Scheme 2. Excitation at 437 nm, where light absorption is dominated by $[\text{Ru}_a^{\text{II}}-\text{O}]^{4+}$, gave the same transient response (Figure 5). The diminished contribution of the $[\text{Ru}_a^{\text{II}}-\text{O}]^{4+}$ bleach at ~445 nm in **1** suggests that >90% of the photochemically generated injection events result in oxidation of the remote catalyst site. The positive feature at ~650 nm that appears following both 437 and 532 nm excitation is

attributable to noninjecting residual excited states (Figures S10 and S11[SI]).



Injection. As previously described, injection yields were determined on the basis of the amplitudes of transient absorption changes.³⁶ Electron injection efficiencies for TiO₂-1 approach ~30% when excited at 440 nm (Table 1). At this wavelength, light absorption is dominated by $[\text{Ru}_a^{\text{II}}-\text{O}]^{4+}$. Excitation at 532 nm, with $[-\text{Ru}_b^{\text{II}}-\text{OH}_2]^{4+}$ the major light absorber, decreases the injection yield to ~12%. The latter is comparable to the injection yield for TiO₂-3 (~15%, Table 1).

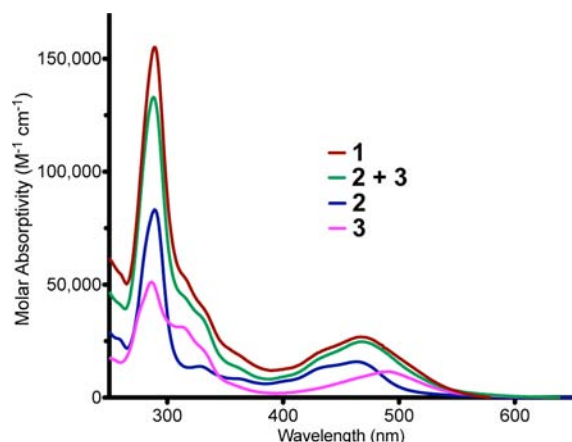


Figure 6. Absorption spectra for 1 (red), 2 (blue), 3 (pink), and 2 + 3 (green) in H₂O at 25 °C.

Table 1. Injection Yields and Back Electron Transfer Rates

complex	Φ_{inj}^a		back electron transfer ^b	
	440 nm excitation	532 nm excitation	τ (μ s)	β
1	0.30	0.12	6.7	0.25
2	0.45	0.44	1.8	0.29
3	0.40	0.15	2.2	0.22

^aSee text. ^b532 nm excitation with monitoring at 480 nm in 0.1 M HClO₄.

440 nm excitation of [TiO₂-Ru^{II}]²⁺ (TiO₂-2) resulted in an injection yield of ~45%. By comparison, the injection efficiency is ~1 for [Ru(4,4'-(PO₃H₂)₂bpy)₂(bpy)]²⁺ (PO₃H₂-bpy = [2,2'-bipyridine]-4,4'-diylidiphosphonic acid), with the phosphate groups directly bound to the bpy.³⁶

Back Electron Transfer. Back electron transfer between the injected electron in TiO₂ (TiO₂(e⁻)) and the oxidized Ru(III) site, [TiO₂(e⁻)-Ru^{II}-Ru^{III}-OH₂]⁴⁺ for 1 (eq 2), [TiO₂(e⁻)-Ru^{III}]²⁺ for 2, and [TiO₂(e⁻)-Ru^{III}-OH₂]²⁺ for 3, was monitored at 480 nm for 1 and 3 and at 450 nm for 2 following laser flash excitation at 532 nm. As found in earlier studies, back electron transfer kinetics are complex and nonexponential.^{36,40} Absorbance–time traces (Figure 7) could

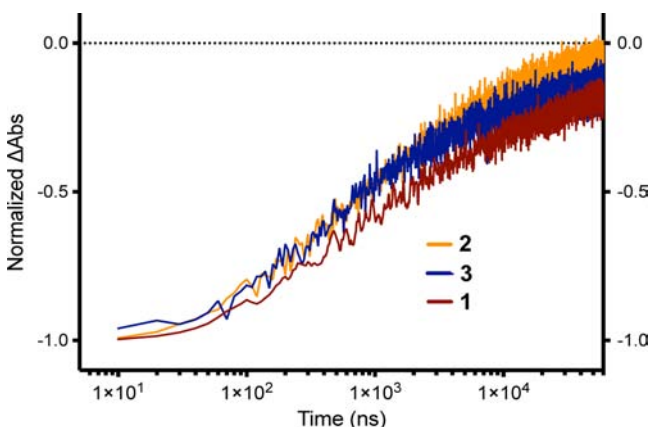
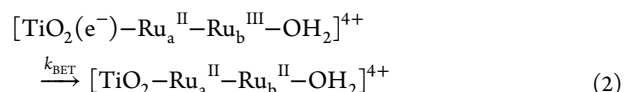


Figure 7. Absorption–time traces for 1 on TiO₂ (4.4×10^{-8} mol cm⁻², red, 480 nm monitoring), 2 (5.8×10^{-8} mol cm⁻², orange, 460 nm monitoring) and 3 (9.1×10^{-8} mol cm⁻², blue, 480 nm monitoring) following 532 nm laser (5.2 mJ) excitation.

be satisfactorily fit to the stretched exponential function (eq 3), where A is a pre-exponential constant, τ is the characteristic lifetime, and β is a parameter that is inversely related to the width of the underlying Lévy distribution of lifetimes, $0 < \beta < 1$.^{41,42} Lifetimes and β values are presented in Table 1 with τ the inverse of the characteristic rate constant for back electron transfer in the distribution, k_{BET} . The lifetimes for 1, 2, and 3 are 6.7, 1.8, and 2.2 μ s, respectively. For a 100 μ s time window, ~5% of the total ΔA change remained for TiO₂-2 and ~10% for TiO₂-1 and TiO₂-3 although back electron transfer for TiO₂-1 is slower initially (Table 1, Figure 7).



$$\Delta\text{OD} = Ae^{-(t/\tau)^\beta} \quad (3)$$

Intra-assembly electron transfer following photochemically generated electron injection of the chromophore in TiO₂-1 (k_{int} , eq 1 and eq 6C) is at least 3 orders of magnitude more rapid than the rate of back electron transfer in [TiO₂(e⁻)-Ru_a^{II}-Ru_b^{III}-OH₂]⁴⁺ (eq 2) at pH = 1 with $k_{BET} \approx 10^5$ ($k_{BET} = 1/\tau$) and $k_{int} > 10^8$. Back electron transfer rates were also found to be dependent on pH although the data at higher pH could not be satisfactorily fit to eq 3. Rather, the time-dependent data are reported as time for half of the total absorbance change to occur ($t_{1/2}$). As can be seen in the data in Table 2, $t_{1/2}$ increases from $t_{1/2} = 6$ μ s at pH = 1 to $t_{1/2} = 35$ μ s at pH = 4.5 (Figure 8, Table 2).

Table 2. pH Dependence of Back Electron Transfer of 1 on TiO₂

sample	BET $t_{1/2}$ (μ s)	>2 ms component ^c (%)
1 pH = 1 ^a	6	6
1 pH = 4.5 ^b	35	23

^a0.1 M HClO₄ at room temperature. ^b0.18 M LiClO₄ with 20 mM pH 4.5 NaOAc/HOAc buffer. ^c% of the ΔA change remaining after 2 ms. Surface coverage: $(6.7 \pm 0.1) \times 10^{-8}$ mol cm⁻²; 532 nm (5.0 mJ) excitation.

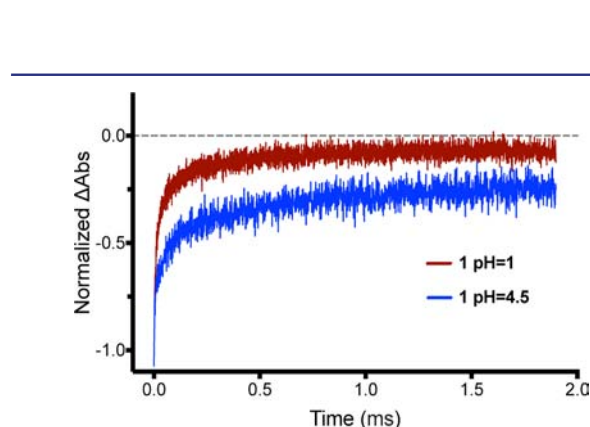


Figure 8. Absorbance–time traces for 1 on TiO₂ (4.4×10^{-8} mol cm⁻²) following 532 nm laser flash (5.0 mJ) excitation with monitoring at 480 nm in 0.1 M HClO₄ (red) and at pH = 4.5 (0.18 M LiClO₄ with 20 mM NaOAc/HOAc buffer) (blue).

DISCUSSION

The goal of this research was to develop a systematic approach for the synthesis of metal oxide-bound chromophore–catalyst assemblies used in the fabrication of photoanodes in DSPECs. The current assembly offers the advantage of relative stability of surface binding under aqueous conditions based on the phosphonate–surface links and a flexible amide link between the chromophore and catalyst. The latter creates a basis for introducing controlled molecular spacers and, with it, a foundation for controlling rates of intramolecular and interfacial electron transfer.

With these goals in mind, the current results provide the basis for what will be a systematic study of the influence of intra-assembly distance effects on intra-assembly and interfacial electron transfer dynamics in DSPEC photoanode applications. These dynamics ultimately dictate the performance of the DSPEC solar fuel half reactions. Achieving high efficiencies in driving multielectron, multiproton solar fuel half reactions, like water oxidation, requires high per photon electron injection efficiencies, stepwise accumulation of multiple oxidative equivalents, and rates of substrate oxidation that exceed rates of back electron transfer. The demands are greater than for conventional DSSCs where photopotential and photocurrents are generated by single photon, single electron events. Even in these cells, efficiencies are still limited by the recombination of $\text{TiO}_2(\text{e}^-)$ with the oxidized form of added redox mediator couples, such as I_3^- .

Synthesis. We report here the development of a general and flexible synthetic strategy for preparing amide linked chromophore–catalyst assemblies with a phosphonate-derivatized chromophore for attachment to oxide surfaces. As previously mentioned, only one other report describes a molecular chromophore–catalyst assembly derivatized with phosphonic acids making the synthetic aspects notable.³⁷ Direct amide coupling between the preformed chromophore and catalyst was unsuccessful due to limited solubility of the phosphonate-derivatized chromophore under conditions relevant to amide coupling. This required a strategy that avoided the phosphonated-bipyridine ligands until the final step in the synthesis (Scheme 1).

An advantage of this procedure is that the $[\text{Ru}(\text{bpy})(\text{Bz})(\text{Cl})]^+$ -analogue intermediate (**7**) is synthesized in high yields without requiring chromatography (see the Experimental Section). In addition, the Cl^- ligands can be replaced with the more labile triflate ligand (OTf^-) to facilitate substitution and for subsequent addition of the phosphonated-bipyridines to build the chromophore. The structure of the triflate-benzene intermediate **8** was evaluated by use of COSY NMR, which identified the $-\text{CH}_2-$ methylene and NH protons, confirming the presence of the amide link after the reaction with HOTf (Figure 3, Scheme 1). Two keys to avoiding hydrolysis of the amide link under the highly acidic conditions used in the synthesis of **8** are the use of anhydrous solvents and controlled temperature. Avoidance of hydrolysis was also a consideration in the use of anhydrous ethylene glycol in the synthesis of **1** in the reaction with the prehydrolyzed ligand ([2,2'-bipyridine]-4,4'-diylbis(methylene)diphosphonic acid). This is an important element since it eliminates the need for hydrolysis of a precursor ester once the ligand has been coordinated.⁴³

Electrochemistry. All three observable oxidations of **1** on FTO in aqueous solution are pH dependent (Figures 4 and S8 [SI]). The introduction of a pH dependence for the

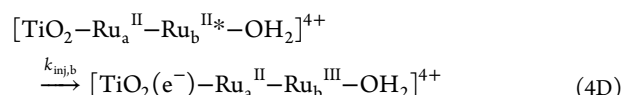
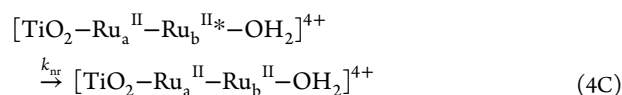
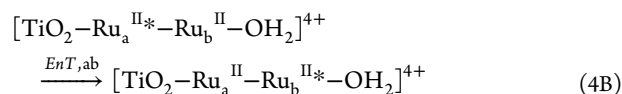
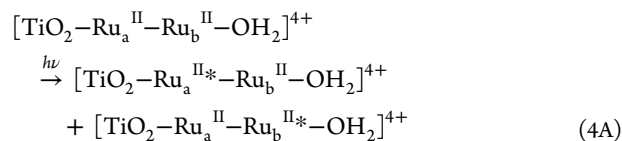
chromophore oxidation $[\text{Ru}_a^{\text{III}}-]^{5+}/[\text{Ru}_a^{\text{II}}-]^{4+}$, in contrast to **4**, arises from a combination of deprotonation of acidic protons on the phosphonic acid groups and the influence of the local electric field gradient at the electrode interface.^{37,44–48} The dependence of 13 mV/pH unit for the $[\text{Ru}_a^{\text{III}}-]^{5+}/[\text{Ru}_a^{\text{II}}-]^{4+}$ couple is in good agreement with earlier observations on surface-bound complexes of the type $[\text{Ru}(\text{bpy})_{3-n}(\text{PO}_3\text{H}_2\text{-CH}_2\text{-bpy})_n]^{2+}$ with $n = 1-3$.⁴⁴ The proton-coupled electron transfer (PCET) oxidations, $[\text{Ru}_a^{\text{II}}-\text{Ru}_b^{\text{III}}-\text{OH}]^{4+}/[\text{Ru}_a^{\text{II}}-\text{Ru}_b^{\text{II}}-\text{OH}_2]^{4+}$ and $[\text{Ru}_a^{\text{II}}-\text{Ru}_b^{\text{IV}}=\text{O}]^{4+}/[\text{Ru}_a^{\text{II}}-\text{Ru}_b^{\text{III}}-\text{OH}]^{4+}$, occur with pH dependences of ~ 74 mV/pH unit, which appears to be the sum of the expected Nernstian behavior (59 mV/pH unit) and the pH dependence of the chromophore $[\text{Ru}_a^{\text{III}}-]^{5+}/[\text{Ru}_a^{\text{II}}-]^{4+}$ couple (13 mV/pH unit).^{49,50}

Interfacial Dynamics. Scheme 2 provides an overview illustrating the complex sequence of energy and electron transfer events expected to occur following MLCT excitation of TiO_2 -**1**.³³ The scheme is based on the absorption spectrum and the various, low-lying MLCT excited states that are accessible at the $[\text{Ru}_a^{\text{II}}-]^{4+}$ and $[-\text{Ru}_b^{\text{II}}-\text{OH}_2]^{4+}$ sites in **1**.

A more detailed, ultrafast photophysical investigation is currently being undertaken, but our experiments on the nanosecond time scale provide significant insight into the dynamics of the events that occur following MLCT excitation at 440 and 532 nm.

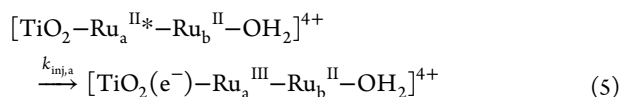
Injection. For TiO_2 -**1** in 0.1 M HClO_4 , the injection yield, following 440 nm excitation, with $[\text{Ru}_a^{\text{II}}-]^{4+}$ the dominant light absorber, is $\eta_{\text{inj}} \approx 0.30$. η_{inj} falls to 0.12 with 532 nm excitation with $[-\text{Ru}_b^{\text{II}}-\text{OH}_2]^{4+}$ as the dominant light absorber. These values, obtained by transient absorbance measurements at the MLCT bleach minimum at 480 nm, are low relative to TiO_2 -**2** with $\eta_{\text{inj}} \approx 0.45$ under the same conditions.

The lower injection efficiencies of TiO_2 -**1** relative to TiO_2 -**2** are presumably due to competitive light absorption by the remote $[-\text{Ru}_b^{\text{II}}-\text{OH}_2]^{4+}$ site. Injection by the excited state $[-\text{Ru}_b^{\text{II}*}-\text{OH}_2]^{4+}$ is expected to be slower because of weak electronic coupling with TiO_2 acceptor levels and a higher medium reorganization energy for electron transfer, which is also distance dependent. Loss of this excited state is dominated by nonradiative decay, eq 4C.³⁸ Intra-assembly energy transfer to give the lowest energy, remote MLCT excited state, $[\text{Ru}_a^{\text{II}}-(\text{H})\text{N}(\text{CO})\text{trpy}^-\bullet]\text{Ru}_b^{\text{III}}-\text{OH}_2]^{4+}$, eq 4B, was found to be much slower than injection in **4** and is not expected to decrease injection yields.³³



By inference, injection by $[\text{TiO}_2-\text{Ru}_a^{\text{II}*}-]^{4+}$ is relatively efficient, eq 5, with some loss to competitive light absorption by

$[-\text{Ru}_b^{\text{II}*}-\text{OH}_2]^{4+}$, eq 4C. Injection from $\text{TiO}_2\text{-3}$ is also wavelength dependent. A higher injection efficiency is observed for the surface attached $\text{Ru}^{\text{III}}(\pi_{\text{bpy}}^*)^1$ excited state, which dominates absorption at 440 nm compared to 532 nm where light absorption gives dominantly a $\text{Ru}^{\text{III}}(\pi_{\text{rpy}}^*)^1$ excited state oriented away from the interface.

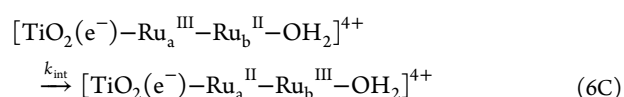
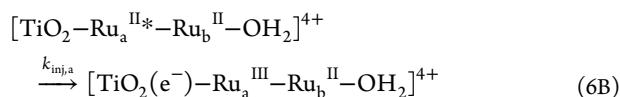
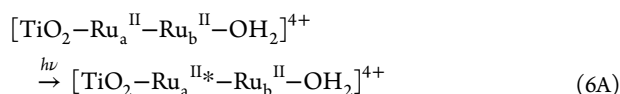


There is an additional loss in injection efficiency for both $\text{TiO}_2\text{-1}$ and $\text{TiO}_2\text{-2}$ due to the $-\text{CH}_2-$ methylene spacers that intervene between the phosphonate groups linked to the TiO_2 surface and the injecting $-\text{CH}_2-(\text{bpy}^*)\text{Ru}^{\text{III}}$ chromophore. Under comparable conditions, $\eta_{\text{inj}} \approx 1$ for $\text{TiO}_2\text{-}[\text{Ru}(4,4'-(\text{PO}_3\text{H}_2)_2\text{bpy})_2(\text{bpy})]^{2+}$ with no methylene spacers.³⁶ Related observations have been made for injection by a family of phosphonate-derivatized Ru-bpy complexes on TiO_2 .⁴⁰

The origin of this effect is not clear but it has been suggested that there may be contributions from decreased electronic coupling between the MLCT excited state(s) and surface acceptor levels and/or from the substituent effect of the $-\text{CH}_2-$ spacers. By their electron-donating effect these spacers direct the lowest MLCT excited state toward the amide-derivatized bridging ligand and away from the interface with TiO_2 .⁴⁰

Excitation at 532 nm with $[-\text{Ru}_b^{\text{II}}-\text{OH}_2]^{4+}$ as the dominant light absorber results in the same transient behavior with the intermediate state $[\text{TiO}_2(e^-)-\text{Ru}_a^{\text{II}}-\text{Ru}_b^{\text{III}}-\text{OH}_2]^{4+}$, appearing in transient spectra but with a considerably diminished electron injection efficiency as described above. The appearance of $[\text{TiO}_2(e^-)-\text{Ru}_a^{\text{II}}-\text{Ru}_b^{\text{III}}-\text{OH}_2]^{4+}$ at this excitation wavelength may include a contribution from long-range $[\text{TiO}_2-\text{Ru}_a^{\text{II}}-\text{Ru}_b^{\text{II}*}-\text{OH}_2]^{4+}$ electron injection, but is probably dominated by electron injection from the minority light absorber, $[\text{TiO}_2-\text{Ru}_a^{\text{II}*}-]^{4+}$ followed by intramolecular electron transfer, eqs 6A–6C.

Intra-Assembly and Back Electron Transfer. Following 440 nm excitation in 0.1 M HClO_4 of $\text{TiO}_2\text{-1}$, with light absorption dominated by $[\text{Ru}_a^{\text{II}}-]^{4+}$, a MLCT bleach appears at 480 nm (Figure 6). The coincidence between this bleach minimum and the bleach minimum for $\text{TiO}_2\text{-3}$ formed by direct injection by 3 into TiO_2 , shows that, at the earliest observation times, MLCT excitation and injection have occurred ($k_{\text{inj},a}$) followed by intra-assembly electron transfer (k_{int}) (eqs 6A–6C). On the basis of this observation, $k_{\text{int}} > 10^8 \text{ s}^{-1}$, making the rate of intra-assembly forward electron transfer at least 3 orders of magnitude greater than the rate of back electron transfer. Also, these results suggest that >90% of injection events are followed by intra-assembly electron transfer oxidation of the water oxidation catalyst site $[-\text{Ru}_b^{\text{II}}-\text{OH}_2]^{4+}$ in 1 (eq 6C).



On the basis of $\text{p}K_a = 1.4$ for $[-\text{Ru}_b^{\text{III}}-\text{OH}_2]^{5+}$ the distribution between the aquo, $[\text{Ru}_a^{\text{II}}-\text{Ru}_b^{\text{III}}-\text{OH}_2]^{5+}$, and hydroxo, $[\text{Ru}_a^{\text{II}}-\text{Ru}_b^{\text{III}}-\text{OH}]^{4+}$, forms of the catalyst in 0.1 M HClO_4 is $[\text{Ru}_a^{\text{II}}-\text{Ru}_b^{\text{III}}-\text{OH}_2]^{5+}/[\text{Ru}_a^{\text{II}}-\text{Ru}_b^{\text{III}}-\text{OH}]^{4+} \approx 2.5$.³⁹ Absorptivity differences between the two forms in the visible are too small to distinguish between them (Figure S12 [SI]). This is also evident in the fact that the transient spectrum at $\text{pH} = 4.5$, where the aquo ligand should be deprotonated after oxidation to give $[\text{TiO}_2(e^-)-\text{Ru}_a^{\text{II}}-\text{Ru}_b^{\text{III}}-\text{OH}]^{4+}$, matches the transient spectrum at $\text{pH} = 1$ (Figure S12 [SI]).

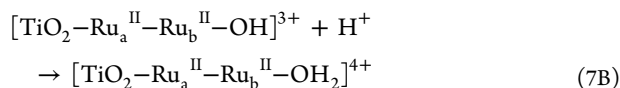
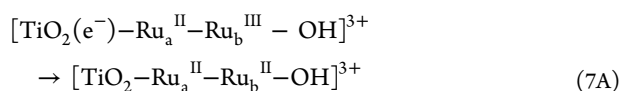
Back electron transfer from $\text{TiO}_2(e^-)$ is typically dictated in whole or part by intrafilm dynamics with recombination rates dependent on the density of electrons in TiO_2 . In these experiments total absorption changes for 1, 2, and 3 at the probe wavelength were -0.030 OD , -0.032 OD , and -0.040 OD , respectively, with the first 100 ns of data omitted to avoid contributions from residual excited states. On the basis of the molar extinction coefficient changes, the electron concentration ratios for 1, 2, and 3 following injection were $\sim 1:0.8:1.3$, respectively, with comparable electron densities for the three.

The results of earlier studies revealed that, for 2 and related back electron transfer rates following electron injection are dominated by electron diffusion through a distribution of trap states in the TiO_2 nanoparticles in TiO_2 films as described by the multiple trapping model.^{36,51,52} This conclusion was reinforced by the results of a recent study on a series of phosphonate-derivatized chromophores on TiO_2 .⁴⁰ The increased spatial separation in the assembly between the surface $\text{TiO}_2(e^-)$ and the remote $[-\text{Ru}_b^{\text{III}}-\text{OH}_2]^{4+}$ increases the through-bond separation distance for back electron transfer and, with it, both the extent of electronic coupling and, to a lesser extent, the outer-sphere barrier to electron transfer. The latter is also distance dependent.^{53–56}

These factors are expected to decrease rates of back electron transfer between $\text{TiO}_2(e^-)$ and $[-\text{Ru}_b^{\text{III}}-\text{OH}_2]^{4+}$ in the surface-bound assembly. However, the decrease for $[\text{TiO}_2(e^-)-\text{Ru}_a^{\text{II}}-\text{Ru}_b^{\text{III}}-\text{OH}_2]^{4+} \rightarrow [\text{TiO}_2-\text{Ru}_a^{\text{II}}-\text{Ru}_b^{\text{II}}-\text{OH}_2]^{4+}$ (1) compared to $[\text{TiO}_2(e^-)-\text{Ru}^{\text{III}}-\text{OH}_2]^{2+} \rightarrow [\text{TiO}_2-\text{Ru}^{\text{II}}-\text{OH}_2]^{2+}$ (3) is only a factor of ~ 3 less with a decrease from 2 to 6.7 μs for the characteristic lifetime, Table 1. The fact that these rates are comparable suggests that the two rates, intrafilm electron transfer and intra-assembly back electron transfer (eq 2), are kinetically coupled.

The rate of back electron transfer is also pH dependent as observed in our previous study on $[\text{TiO}_2(e^-)-\text{Ru}^{\text{III}}]^{2+} \rightarrow [\text{TiO}_2-\text{Ru}^{\text{II}}]^{2+}$ back electron transfer for $[\text{Ru}(4,4'-(\text{PO}_3\text{H}_2)_2\text{bpy})_2(\text{bpy})]^{2+}$.³⁶ A pH dependence is qualitatively consistent with the multiple-state trapping model and the expected influence of $\text{pH}^{51,52}$ although the decrease is only a factor of 2 between pH 1 and 5.³⁶ For $\text{TiO}_2\text{-1}$, there is a decrease by a factor of ~ 6 in $t_{1/2}$ from 6 to 35 μs between $\text{pH} = 1$ and 4.5, pointing to an additional effect.

At $\text{pH} = 4.5$, the oxidized assembly undergoes deprotonation to $[\text{TiO}_2(e^-)-\text{Ru}_a^{\text{II}}-\text{Ru}_b^{\text{III}}-\text{OH}]^{3+}$ with a $\text{p}K_a \approx 1.4$ for $[-\text{Ru}_b^{\text{III}}-\text{OH}_2]^{4+}$.³³ On the basis of the $E_{1/2}$ values in Figure 4, back electron transfer for the hydroxyl form of the assembly, eq 7A, is thermodynamically less favorable than reduction of $[-\text{Ru}_b^{\text{III}}-\text{OH}_2]^{4+}$, which also contributes to the decrease in rate, eq 7.



Another observation of note is the increase in the fraction of ΔOD change that persists to 2 ms from 6% at pH = 1 to 23% at pH = 4.5. Maintaining redox equivalents on the millisecond and longer time scales is an essential element for building up the multiple redox equivalents required to drive multiple electron solar fuel half reactions.

CONCLUSIONS

We present here a general synthetic strategy for preparing a class of amide-linked, chromophore–water oxidation catalyst assemblies derivatized with phosphonate groups for binding to oxide surfaces. Analysis of interfacial dynamics for $\text{TiO}_2\text{-I}$ by nanosecond transient absorption measurements demonstrates that excitation and injection are followed by rapid oxidation of the remote catalyst site to give $[\text{TiO}_2(\text{e}^-)\text{-Ru}_a^{\text{II}}\text{-Ru}_b^{\text{III}}\text{-OH}_2]^{4+}$. Electron injection efficiencies are wavelength dependent consistent with inefficient injection by the remote $[-\text{Ru}_b^{\text{II}*}\text{-OH}_2]^{4+}$ excited state. Following injection and intra-assembly electron transfer, back electron transfer from $\text{TiO}_2(\text{e}^-)$ to the remote $[-\text{Ru}_b^{\text{III}}\text{-OH}_2]^{4+}$ site is kinetically dictated by an interplay between intrafilm and $\text{TiO}_2(\text{e}^-) \rightarrow [-\text{Ru}_b^{\text{III}}\text{-OH}_2]^{4+}$ back electron transfer dynamics. At least 90% of the photochemically generated injection events are followed by rapid intra-assembly electron transfer to generate a remote oxidized catalyst site at $[-\text{Ru}_b^{\text{III}}\text{-OH}_2]^{4+}$. The rate of back electron transfer at pH = 4.5, following deprotonation to give $[-\text{Ru}_b^{\text{III}}\text{-OH}]^{3+}$, is further decreased by a factor of ~ 4 compared to pH = 1.

EXPERIMENTAL SECTION

Materials. $[\text{Ru}(\eta^6\text{-Bz})(\text{Cl})_2]_2$,⁵⁷ (4'-methyl-[2,2'-bipyridin]-4-yl)-methanamine,³³ ([2,2'-bipyridine]-4,4'-diylbis(methylene)) diphosphonic acid,⁴³ $\text{Ru}(\text{trpy})\text{Cl}_3$,⁵⁸ $[\text{Ru}(\eta^6\text{-Bz})(2,2'\text{-bipyridine})(\text{Cl})](\text{Cl})$,⁴³ and $[\text{Ru}(\text{trpy})(\text{PO}_3\text{H}_2\text{-CH}_2\text{-bpy})(\text{OH}_2)]^{2+}$ (3)^{59,60} were synthesized as reported previously.

4-([2,2':6',2''-Terpyridin]-4'-yl)benzoic Acid. This ligand was prepared by a modified literature procedure.⁶¹ 4-Formylbenzoic acid (5.57 g, 37.1 mmol) was dissolved in ~ 120 mL ethanol. To this mixture was added 1-(pyridin-2-yl)ethanone (8.55 g, 70.6 mmol) and 6 mL of concentrated NH_4OH followed by the addition of NaOH (2.5 g) dissolved in ~ 6 mL of H_2O . The reaction was stirred open to the air at 40 °C overnight during which time a white precipitate began to form. The reaction was cooled, and the precipitate was collected to give clean 4-([2,2':6',2''-terpyridin]-4'-yl)benzoic acid (5.5 g). Allowing the filtrate to sit for an additional day yielded more precipitate, which yielded additional product (2.5 g). This compound was used without further purification (8.0 g, 61.0%). ¹H NMR (600 MHz, $\text{DMSO-}d_6$): δ (ppm) 8.76 (d, 2H), 8.72 (s, 2H), δ 8.64 (d, 2H), δ 8.07 (d, 2H), δ 8.04 (dt, 2H), δ 7.83 (d, 2H), δ 7.52 (dd, 2H). HR-ESI-MS: $m/z = 354.1234^{1+}$, $[\text{M} + \text{H}^+]^{1+} = 354.1243$.

[Ru(4-([2,2':6',2''-Terpyridin]-4'-yl)benzoic acid)(bpy)(Cl)Cl] (5). $[\text{Ru}(\text{bpy})(\eta^6\text{-Bz})(\text{Cl})]\text{Cl}$ (1.75 g, 4.31 mmol) and 4-([2,2':6',2''-terpyridin]-4'-yl)benzoic acid (1.52 g, 4.30 mmol) were heated at reflux for 20 min at 160 °C in ~ 40 mL of 1:1 EtOH: H_2O in a microwave oven. The solution was cooled, filtered, and concentrated on a rotary evaporator. The dark-red solid was triturated with ether, collected, and air dried (2.89 g, 98%). This complex was used without further purification.¹ ¹H NMR and mass spectrometric analysis match

those of the previously reported complex.³³ ¹H NMR (600 MHz, $\text{DMSO-}d_6$): δ (ppm) 10.1 (d, 1H), 9.27 (s, 2H), 8.99 (d, 2H), 8.95 (d, 1H), 8.66 (d, 1H), 8.48 (d, 2H), 8.39 (t, 1H), 8.22 (d, 2H), 8.07 (t, 1H), 8.02 (t, 2H), 7.78 (t, 1H), 7.63 (d, 2H), 7.41 (m, 3H), 7.08 (t, 1H). HR-ESI-MS: $m/z = 646.0572^{1+}$, $[\text{M}]^{1+} = 646.0584$.

[Ru(bpy-ph-NH-CO-trpy)(bpy)(Cl)]PF₆ (6). $[\text{Ru}(4\text{-}([2,2':6',2''\text{-terpyridin}]\text{-4'-yl)benzoic acid})(\text{bpy})(\text{Cl})]\text{Cl}$ (2 g, 2.93 mmol) was dissolved in SOCl_2 (10 mL) and heated at reflux under an atmosphere of argon for 4 h. The reaction mixture was cooled to 50 °C and SOCl_2 removed under reduced pressure to yield a dark-red solid. To the same flask was added (4'-methyl-[2,2'-bipyridin]-4-yl)methanamine (0.584 g, 2.93 mmol). The two solids were purged several times with argon followed by addition of anhydrous DMF (20 mL) and anhydrous *N,N*-diisopropylethylamine (DIPEA) (1 mL). The reaction was stirred under argon at 100 °C overnight, the reaction solution was cooled to room temperature, and a saturated solution of NH_4PF_6 (5 mL) was added with 50 mL of H_2O . The suspension was stirred for several hours to ensure complete precipitation. The solid was collected, washed with water and ether, and air dried (2.7 g, 97%). This complex was used without further purification. The trpy-bpy protons of the Ru complex are sharp, but the free bipyridine peaks are broad due to the fluxional behavior of the ligand on the NMR time scale. ¹H NMR (600 MHz, $\text{DMSO-}d_6$): δ (ppm) 10.1 (d, 1H), 9.47 (bs, 1H), 9.26 (s, 2H), 8.96 (d, 2H), 8.93 (d, 1H), 8.80 (bs, 2H), 8.65 (bd, 2H), 8.44 (d, 1H), 8.35 (m, 2H), 8.23 (d, 2H), 8.05 (m, 3H), 7.78 (t, 1H), 7.63 (d, 2H), 7.39 (m, 3H), 7.29 (bs, 1H), 7.06 (t, 1H), 7.02 (bs, 1H), 4.70 (bs, 2H), 2.43 (bs, 3H). HR-ESI-MS: $m/z = 827.1552^{1+}$, $[\text{M}]^{1+} = 827.1588$.

[Ru(bpy)(Cl)(trpy-bpy)Ru(Bz)(Cl)](Cl)(PF₆) (7). $[\text{Ru}(\text{bpy})(\text{Cl})\text{-}(\text{trpy-bpy})]\text{PF}_6$ (1.49 g, 1.53 mmol) and $[\text{Ru}(\eta^6\text{-Bz})(\text{Cl})_2]_2$ (0.38 g, 0.77 mmol) were heated at reflux in anhydrous methanol overnight under an atmosphere of argon. The reaction was cooled, and the precipitate was collected and washed with methanol and ether. Recrystallization from methanol gave pure product (1.3 g, 70%). This complex was used without further purification. ¹H NMR (600 MHz, $\text{DMSO-}d_6$): δ (ppm) 10.1 (d, 1H), 9.57 (d, 1H), 9.52 (t, 1H), 9.47 (d, 1H), 9.26 (s, 2H), 8.96 (d, 2H), 8.93 (d, 1H), 8.51 (m, 2H), 8.46 (m, 2H), 8.37 (t, 1H), 8.24 (d, 2H), 8.06 (t, 1H), 8.03 (t, 2H), 7.80 (t, 1H), 7.70 (d, 1H), 7.65 (m, 3H), 7.41 (m, 3H), 7.07 (t, 1H), 6.19 (s, 6H), δ 7.77 (dd, 2H), 2.58 (s, 3H). HR-ESI-MS: $m/z = 521.04346^{2+} = 1042.0869$, $[\text{M}]^{2+} = 1042.0789$, $m/z = 1187.03997^{1+}$, $[\text{M} + \text{PF}_6]^{1+} = 1187.0431$.

[Ru(bpy)(OTf)(trpy-bpy)Ru(Bz)(OTf)](OTf)₂ (8). **6** (1.2 g, 0.981 mmol) was suspended in anhydrous dichloromethane (~ 200 mL) and thoroughly degassed with argon. Under a constant flow of argon, with a vent to release HCl gas, triflic acid (~ 2 mL) was added. The suspension was stirred at room temperature under a flow of argon for 4 h. Ether (~ 200 mL) was added, and the precipitate was collected by filtration and washed with ether. This complex was used without further purification (1.52 g, 99%). ¹H NMR (600 MHz, CD_3CN): δ (ppm) 9.65 (d, 1H), 9.35 (d, 1H), 9.23 (d, 1H), 8.91 (s, 2H), 8.77 (bt, 1H), 8.65 (t, 3H), 8.48 (s, 1H), 8.36 (m, 5H), 8.28 (s, 1H), 8.06 (t, 2H), 8.00 (t, 1H), 7.83 (m, 2H), 7.73 (d, 2H), 7.63 (d, 1H), 7.39 (m, 3H), 7.11 (t, 1H), 6.24 (s, 6H), 4.92 (bd, 2H), 2.63 (s, 3H). HR-ESI-MS: $m/z = 387.0457^{3+} = 1161.1371$, $[\text{M} + \text{NCMe} + \text{OTf}]^{3+} = 1161.1210$; $m/z = 580.0759^{2+} = 1160.1518$, $[\text{M} + \text{NCMe} + \text{OTf} - \text{H}^+]^{2+} = 1160.1131$.

[((PO₃H₂-CH₂)₂-bpy)₂Ru(bpy-NH-CO-trpy)Ru(bpy)(OH₂)](OTf)₄ (1). $[\text{Ru}(\text{bpy})(\text{OTf})(\text{trpy-bpy})\text{Ru}(\text{Bz})(\text{OTf})](\text{OTf})_2$ (0.50 g, 0.32 mmol) and ([2,2'-bipyridine]-4,4'-diylbis(methylene))-diphosphonic acid (0.22g, 0.64 mmol) were dissolved in anhydrous ethylene glycol. The reaction was heated to 120 °C for 5 h and followed by UV/vis measurements by watching the growth in absorbance at $\lambda_{\text{max}} \approx 470$ nm. At the end of the reaction period, the solution was cooled to room temperature, and acetone was added. The solution was again brought to reflux, cooled, filtered, and washed with acetone to remove unreacted $[\text{Ru}(\text{bpy})(\text{OTf})(\text{trpy-bpy})\text{Ru}(\text{Bz})(\text{OTf})](\text{OTf})_2$. The solid was then suspended in methanol, brought to reflux, cooled, and filtered to remove any insoluble material. The filtrate was taken to dryness by rotary evaporation, and the crude product was purified by size exclusion chromatography (Sephadex LH-

20 with H₂O as eluent). Similar fractions (based on UV–vis) were combined, and the solvent was removed by rotary evaporation. The dark-red solid was triturated with ether and collected (0.195 g, 28%). ¹H NMR (600 MHz, D₂O): δ (ppm) 9.51 (d, 1H), 9.38 (t, 1H), 8.83 (s, 2H), 8.63 (d, 1H), 8.50 (d, 2H), 8.41 (s, 1H), 8.32 (m, 4H), 8.32 (d, 2H), 8.13 (d, 2H), 8.05 (d, 2H), 7.98 (t, 1H), 7.94 (t, 2H), 7.81 (d, 1H), 7.76 (d, 2H), 7.60 (m, 5H), 7.29 (m, 4H), 7.17 (m, 6H), 6.88 (t, 1H), 3.14 (m, 8H), 2.46 (s, 3H). ³¹P NMR δ 16.88. HR-ESI-MS (80:20 NCMe/H₂O, 1% HCCOH): *m/z* = 540.3945³⁺ = 1621.183, [M – 2H⁺ + Na + H₂O]³⁺ = 1621.144; *m/z* = 548.0544³⁺ = 1644.163 [M – 2H⁺ + Na + NCMe]³⁺ = 1644.160; *m/z* = 810.0856²⁺ = 1620.1712, [M – 3H⁺ + Na + H₂O]²⁺ = 1620.135; *m/z* = 821.57806²⁺ = 1643.1561, [M – 3H⁺ + Na + NCMe]²⁺ = 1643.1525. Anal. Found (Calc) for C₇₀H₈₀F₆N₁₂O₂₉P₄Ru₂S₂: C, 40.38 (40.86); H, 4.16 (3.92); N, 8.32 (8.17).

[Ru(PO₃H₂-CH₂)₂-bpy)₂(dmb)(Cl)₂ (2). This complex was synthesized according to a literature procedure but by using 4,4'-dimethyl-2,2'-bipyridine instead of 2,2'-bipyridine.⁴³ ¹H NMR (400 MHz, D₂O): δ (ppm) 8.35 (bd, 4H), 8.26 (s, 2H), 7.70 (dd, 4H), 7.56 (d, 2H), 7.19 (bt, 4H), 7.12 (d, 2H), 3.01 (d, 8H), 2.47 (s, 6H). ³¹P NMR δ 15.06, 14.93.

Preparation of Modified Electrodes. Titanium isopropoxide, isopropanol, and hydroxypropylcellulose were used as received from Sigma-Aldrich. Fluorine-doped tin oxide (FTO)-coated glass (Hartford Glass Co.; sheet resistance 15 Ω/cm²) was cut into 11 mm × 50 mm strips that were used as substrates for TiO₂ nanoparticle films. ITO electrodes (ITO-coated glass, R_s = 4–8 Ω) were obtained from Delta Technologies, Limited. NanoITO powder was obtained from Lihochem. NanoITO and TiO₂ were prepared as previously reported.^{62–64} Zirconium dioxide was prepared by using a reported literature procedure.³⁸

Assembly 1 was loaded onto TiO₂ surfaces by immersing the metal oxide films in methanol solutions of 1 for 12 h and then thoroughly rinsed with methanol. Surface coverages were calculated by using the expression $\Gamma = A(\lambda)/(\epsilon(\lambda)1000)$. Maximum coverage (Γ_0) on 6 μm thick TiO₂ films was ~6.7 × 10⁻⁸ mol cm⁻².

Electrochemical and Spectroscopic Characterization. UV–visible spectra were recorded on an Agilent-Varian Cary 50 UV/visible spectrophotometer. Electrochemical measurements were conducted by using a CH Instruments 660D potentiostat. The working electrode was a planar FTO electrode derivatized with 1, Pt-wire counter electrode, and a Ag/AgCl reference (3 M NaCl, 0.205 V vs NHE). E_{1/2} values were obtained from the peak currents in differential pulse voltammograms and are reported vs the normal hydrogen electrode (NHE).

Transient Absorption. Transient absorption (TA) measurements were conducted by using nanosecond laser pulses produced by a Spectra-Physics Quanta-Ray Lab-170 Nd:YAG laser combined with a VersaScan OPO (5–7 ns, operated at 1 Hz) integrated into a commercially available Edinburgh LP920 laser flash photolysis spectrometer system. White light probe pulses generated by a pulsed 450 W Xe lamp passed through a 395 nm long pass filter before reaching the sample to avoid direct band gap excitation of TiO₂. For measurement at time scales >100 μs, a tungsten/halogen lamp under continuous wave mode was used for the probe beam. The probe light was focused into the monochromator and then detected by a photomultiplier tube (Hamamatsu R928) for 395–800 nm wavelength range, respectively. Detector outputs were processed by using a Tektronix TDS3032C digital phosphor oscilloscope interfaced to a PC loaded with Edinburgh's L900 software. Single wavelength kinetic data were the result of averaging 30–100 laser shots with the data fit by using either Origin or Edinburgh LP900 software. Transient spectra at fixed delay times following laser excitation were obtained by using a gated CCD (Princeton Instruments, PI-MAX 3) with 10 ns gates.

■ ASSOCIATED CONTENT

Supporting Information

One- and two-dimensional NMR spectra, UV/vis spectra, electrochemistry, and transient absorption spectra. This

material is available free of charge via the Internet at <http://pubs.acs.org>.

■ AUTHOR INFORMATION

Corresponding Author

tjmeyer@unc.edu

Notes

The authors declare no competing financial interest.

■ ACKNOWLEDGMENTS

This work was funded by the UNC Energy Frontier Research Center (EFRC) “Center for Solar Fuels”, an EFRC funded by the U.S. Department of Energy, Office of Science, Office of Basic Energy Sciences under award DE-SC0001011, supporting D.L.A., M.R.N., and Z.F. (T.J.M., J.L.T., J.J.C., M.K.B.). We acknowledge funding by the Army Research Office through Grant W911NF-09-1-0426 supporting C.R.K.G. (T.J.M.). Funding for W.S. (T.J.M.) was provided by the CCHF, an EFRC funded by the U.S. Department of Energy, Office of Science, Office of Basic Energy Sciences, under award number DE-SC0001298 at the University of Virginia. We acknowledge support for the purchase of instrumentation from the UNC EFRC (Center for Solar Fuels, an Energy Frontier Research Center funded by the U.S. Department of Energy, Office of Science, Office of Basic Energy Sciences under award number DE-SC0001011) and UNC SERC (“Solar Energy Research Center Instrumentation Facility” funded by the U.S. Department of Energy, Office of Energy and Efficiency and Renewable Energy under award number DE-EE0003188).

■ REFERENCES

- (1) Lewis, N. S.; Nocera, D. G. *Proc. Natl. Acad. Sci. U.S.A.* **2006**, *103*, 15729.
- (2) Nocera, D. G. *ChemSusChem* **2009**, *2*, 387.
- (3) Concepcion, J. J.; Jurss, J. W.; Brennaman, M. K.; Hoertz, P. G.; Patrocinio, A. O. T.; Murakami Iha, N. Y.; Templeton, J. L.; Meyer, T. J. *Acc. Chem. Res.* **2009**, *42*, 1954.
- (4) Eisenberg, R.; Gray, H. B. *Inorg. Chem.* **2008**, *47*, 1697.
- (5) Wasielewski, M. R. *Acc. Chem. Res.* **2009**, *42*, 1910.
- (6) Renger, G. *Photosynth. Res.* **2007**, *92*, 407.
- (7) Ferreira, K. N.; Iverson, T. M.; Maghlaoui, K.; Barber, J.; Iwata, S. *Science* **2004**, *303*, 1831.
- (8) Stull, J. A.; Stich, T. A.; Service, R. J.; Debus, R. J.; Mandal, S. K.; Armstrong, W. H.; Britt, R. D. *J. Am. Chem. Soc.* **2010**, *132*, 446.
- (9) Meyer, T. J.; Huynh, M. H. V.; Thorp, H. H. *Angew. Chem., Int. Ed.* **2007**, *46*, 5284.
- (10) Huynh, M. H. V.; Dattelbaum, D. M.; Meyer, T. J. *Coord. Chem. Rev.* **2005**, *249*, 457.
- (11) Youngblood, W. J.; Lee, S.-H. A.; Kobayashi, Y.; Hernandez-Pagan, E. A.; Hoertz, P. G.; Moore, T. A.; Moore, A. L.; Gust, D.; Mallouk, T. E. *J. Am. Chem. Soc.* **2009**, *131*, 926.
- (12) Sivasankar, N.; Weare, W. W.; Frei, H. *J. Am. Chem. Soc.* **2011**, *133*, 12976.
- (13) Duan, L.-L.; Xu, Y.-H.; Tong, L.-P.; Sun, L.-C. *ChemSusChem* **2011**, *4*, 238.
- (14) Concepcion, J. J.; Jurss, J. W.; Templeton, J. L.; Meyer, T. J. *Proc. Natl. Acad. Sci. U.S.A.* **2008**, *105*, 17632.
- (15) Tinker, L. L.; McDaniel, N. D.; Bernhard, S. J. *Mater. Chem.* **2009**, *19*, 3328.
- (16) Song, W.; Chen, Z.; Brennaman, M. K.; Concepcion, J. J.; Patrocinio, A. O. T.; Iha, N. Y. M.; Meyer, T. J. *Pure Appl. Chem.* **2011**, *83*, 749.
- (17) Suzuki, H.; Nagasaka, M.; Sugiura, M.; Noguchi, T. *Biochemistry* **2005**, *44*, 11323.

- (18) Miksovská, J.; Schiffer, M.; Hanson, D. K.; Sebban, P. *Proc. Natl. Acad. Sci. U.S.A.* **1999**, *96*, 14348.
- (19) Mueh, F.; Gloeckner, C.; Hellmich, J.; Zouni, A. *Biochim. Biophys. Acta, Bioenerget.* **2012**, *1817*, 44.
- (20) Olson, J. M.; Pierson, B. K. *Int. Rev. Cytol.* **1987**, *108*, 209.
- (21) Barber, J. *Photosynth. Res.* **2004**, *80*, 137.
- (22) Treadway, J. A.; Moss, J. A.; Meyer, T. J. *Inorg. Chem.* **1999**, *38*, 4386.
- (23) Gerischer, H. *Electrochim. Acta* **1993**, *38*, 3.
- (24) Gerischer, H. *Electrochim. Acta* **1995**, *40*, 1277.
- (25) Xu, Y.; Eilers, G.; Borgstroem, M.; Pan, J.; Abrahamsson, M.; Magnuson, A.; Lomoth, R.; Bergquist, J.; Polivka, T.; Sun, L.; Sundstroem, V.; Styring, S.; Hammarstroem, L.; Aakermark, B. *Chem.—Eur. J.* **2005**, *11*, 7305.
- (26) Martinson, A. B. F.; Hamann, T. W.; Pellin, M. J.; Hupp, J. T. *Chem.—Eur. J.* **2008**, *14*, 4458.
- (27) Clifford, J. N.; Martinez-Ferrero, E.; Viterisi, A.; Palomares, E. *Chem. Soc. Rev.* **2011**, *40*, 1635.
- (28) Balzani, V.; Credi, A.; Venturi, M. *ChemSusChem* **2008**, *1*, 26.
- (29) Gust, D.; Moore, T. A.; Moore, A. L. *Acc. Chem. Res.* **2009**, *42*, 1890.
- (30) Concepcion, J. J.; Tsai, M.-K.; Muckerman, J. T.; Meyer, T. J. *J. Am. Chem. Soc.* **2010**, *132*, 1545.
- (31) Concepcion, J. J.; Jurss, J. W.; Templeton, J. L.; Meyer, T. J. *J. Am. Chem. Soc.* **2008**, *130*, 16462.
- (32) Chen, Z.; Concepcion, J. J.; Hu, X.; Yang, W.; Hoertz, P. G.; Meyer, T. J. *Proc. Natl. Acad. Sci. U.S.A.* **2010**, *107*, 7225.
- (33) Ashford, D. L.; Stewart, D. J.; Glasson, C. R.; Binstead, R. A.; Harrison, D. P.; Norris, M. R.; Concepcion, J. J.; Fang, Z.; Templeton, J. L.; Meyer, T. J. *Inorg. Chem.* **2012**, *51*, 6428.
- (34) Hanson, K.; Brennaman, M. K.; Luo, H.; Glasson, C. R. K.; Concepcion, J. J.; Song, W.; Meyer, T. J. *ACS Appl. Mater. Interfaces* **2012**, *4*, 1462.
- (35) Hanson, K.; Ashford, D. L.; Lou, H.; Concepcion, J. J.; Templeton, J. L.; Meyer, T. J. *J. Am. Chem. Soc.* **2012**, *134*, 16975.
- (36) Brennaman, M. K.; Patrocino, A. O. T.; Song, W.-J.; Jurss, J. W.; Concepcion, J. J.; Hoertz, P. G.; Traub, M. C.; Murakami Iha, N. Y.; Meyer, T. J. *ChemSusChem* **2011**, *4*, 216.
- (37) Concepcion, J. J.; Jurss, J. W.; Hoertz, P. G.; Meyer, T. J. *Angew. Chem., Int. Ed.* **2009**, *48*, 9473.
- (38) Song, W.; Glasson, C. R. K.; Luo, H.; Hanson, K.; Brennaman, M. K.; Concepcion, J. J.; Meyer, T. J. *J. Phys. Chem. Lett.* **2011**, *2*, 1808.
- (39) Trammell, S. A.; Wimbish, J. C.; Odobel, F.; Gallagher, L. A.; Narula, P. M.; Meyer, T. J. *J. Am. Chem. Soc.* **1998**, *120*, 13248.
- (40) Hanson, K.; Brennaman, M. K.; Ito, A.; Luo, H.; Song, W.; Parker, K. A.; Ghosh, R.; Norris, M. R.; Glasson, C. R. K.; Concepcion, J. J.; Lopez, R.; Meyer, T. J. *J. Phys. Chem. C* **2012**, *116*, 14837.
- (41) Lindsey, C. P.; Patterson, G. D. *J. Chem. Phys.* **1980**, *73*, 3348.
- (42) Williams, G.; Watts, D. C. *Trans. Faraday Soc.* **1970**, *66*, 80.
- (43) Norris, M. R.; Concepcion, J. J.; Glasson, C. R. K.; Ashford, D. L.; Templeton, J. L.; Meyer, T. J. In preparation.
- (44) Jurss, J. W.; Binstead, R. A.; Norris, M. R.; Concepcion, J. J.; Templeton, J. L.; Meyer, T. J. In preparation.
- (45) Qu, P.; Meyer, G. J. *Langmuir* **2001**, *17*, 6720.
- (46) Zaban, A.; Ferrere, S.; Gregg, B. A. *J. Phys. Chem. B* **1998**, *102*, 452.
- (47) van der Vegte, E. W.; Hadziioannou, G. *J. Phys. Chem. B* **1997**, *101*, 9563.
- (48) Yan, S. G.; Hupp, J. T. *J. Phys. Chem.* **1996**, *100*, 6867.
- (49) Wasylenko, D. J.; Ganesamoorthy, C.; Henderson, M. A.; Koivisto, B. D.; Osthoff, H. D.; Berlinguette, C. P. *J. Am. Chem. Soc.* **2010**, *132*, 16094.
- (50) Concepcion, J. J.; Jurss, J. W.; Norris, M. R.; Chen, Z.; Templeton, J. L.; Meyer, T. J. *Inorg. Chem.* **2010**, *49*, 1277.
- (51) Anta, J. A.; Nelson, J.; Quirke, N. *Phys. Rev. B: Condens. Matter* **2002**, *65*, 125324/1.
- (52) Nelson, J.; Chandler, R. E. *Coord. Chem. Rev.* **2004**, *248*, 1181.
- (53) Bonhote, P.; Moser, J.-E.; Humphry-Baker, R.; Vlachopoulos, N.; Zakeeruddin, S. M.; Walder, L.; Graetzel, M. *J. Am. Chem. Soc.* **1999**, *121*, 1324.
- (54) Clifford, J. N.; Palomares, E.; Nazeeruddin, M. K.; Graetzel, M.; Nelson, J.; Li, X.; Long, N. J.; Durrant, J. R. *J. Am. Chem. Soc.* **2004**, *126*, 5225.
- (55) Hirata, N.; Lagref, J.-J.; Palomares, E. J.; Durrant, J. R.; Nazeeruddin, M. K.; Gratzel, M.; Di Censo, D. *Chem.—Eur. J.* **2004**, *10*, 595.
- (56) Serron, S. A.; Aldridge, W. S., III; Fleming, C. N.; Danell, R. M.; Baik, M.-H.; Sykora, M.; Dattelbaum, D. M.; Meyer, T. J. *J. Am. Chem. Soc.* **2004**, *126*, 14506.
- (57) Bennett, M. A.; Smith, A. K. *J. Chem. Soc., Dalton Trans.* **1974**, 233.
- (58) Sullivan, B. P.; Calvert, J. M.; Meyer, T. J. *Inorg. Chem.* **1980**, *19*, 1404.
- (59) Kiyota, J.; Yokoyama, J.; Yoshida, M.; Masaoka, S.; Sakai, K. *Chem. Lett.* **2010**, *39*, 1146.
- (60) Gallagher, L. A.; Meyer, T. J. *J. Am. Chem. Soc.* **2001**, *123*, 5308.
- (61) Constable, E. C.; Dunphy, E. L.; Housecroft, C. E.; Neuburger, M.; Schaffner, S.; Schaper, F.; Batten, S. R. *Dalton Trans.* **2007**, 4323.
- (62) Chen, Z.; Concepcion, J. J.; Hull, J. F.; Hoertz, P. G.; Meyer, T. J. *Dalton Trans.* **2010**, *39*, 6950.
- (63) Hoertz, P. G.; Chen, Z.; Kent, C. A.; Meyer, T. J. *Inorg. Chem.* **2010**, *49*, 8179.
- (64) Lee, S.-H. A.; Abrams, N. M.; Hoertz, P. G.; Barber, G. D.; Halaoui, L. I.; Mallouk, T. E. *J. Phys. Chem. B* **2008**, *112*, 14415.